SAND2011-9398 C

SAND2011-9398C

Correlating Pit Initiation in Aluminum with Passive Oxide Defect Structure

K.R. Zavadil

Sandia National Laboratories, Albuquerque, New Mexico, 87185-0888, USA

Microelectrochemical methods are combined with scanning electron microscopy to explore passive oxide breakdown and pit initiation on Al(111) thin films. Anodic galvanostatic polarization is conducted in a microcapillary cell to limit the available current and to restrict the analysis area for subsequent microscopic evaluation. An ability to drive a single pit initiation event is demonstrated using this approach. Subsequent microscopy shows that pore cluster formation on the off-(111) axis facets that are emergent from the grain boundaries is responsible for pit initiation. Early stage, fully formed pits possess oxide membranes that contain pore clusters. Pores evolve from voids that form at the oxide-Al interface, establishing a link between these interfacial voids and pit initiation. Localized oxygen vacancy saturation and the anion-cation vacancy annihilation reaction during anodic polarization drive void growth, the void-to-pore transition, and pit initiation at off-(111) axis facets in this system.

Introduction

Pit initiation is considered to be a first step in a number of localized corrosion processes leading to accumulated damage for a wide range of passive metals and alloys. The origin of pit initiation has been the subject of study for decades within the corrosion community (1-3). A number of descriptive mechanisms have been proposed for passivity breakdown in pure metals (4-8), along with the detection and characterization of early stage processes including pit nucleation (9) and metastable pitting (10). However, a definitive chemical and physical description of the initiation site and its evolution does not exist to aid in validating both the community's understanding of mechanism and the resulting models used to describe the pitting process. Successful site description provides the opportunity to create such initiation sites, electrochemically interrogate these sites through environmental control, and establish causal relationships with pitting. This study focuses on developing a relationship between voids, demonstrated to form at the oxide-aluminum interface with anodic polarization in aqueous media (11), and the eventual initiation of a pit.

Metallic films of aluminum represent a convenient substrate with which to explore pit initiation. Well defined, reproducible films in terms of composition, grain size and orientation, and oxide characteristics are readily deposited onto silicon substrates. Pitting in aluminum thin films has been explored previously to develop the relationships between film thickness, evolving pit geometry, the repassivation potential and critical current density necessary to drive propagation (12). The intent of the current study is to explore the role of the oxide on pit initiation and to therefore limit the extent of propagation. One method of accomplishing restricted propagation is to operate in a controlled current or

galvanostatic mode where the critical current density necessary to grow a pit is rapidly exceeded once pit initiation takes place.

The work presented in this paper demonstrates that anodic galvanostatic polarization is effective at driving single pit initiation events. When applied as a microelectrochemical technique, electron microscopic imaging of early stage pits and pit precursor sites becomes a viable characterization strategy because of the small size of the polarized region. The application of 4 to 14 $\mu A \cdot cm^{-2}$ current density to a 3 $x10^{-6}$ cm^2 region of an Al(111) textured film surface is sufficient to drive pit initiation but limit the growth of the resulting pit. Localization of current results in the creation of clusters of closely spaced pores that preferentially form on the off-(111) axis facets emergent from the grain boundary. Fully formed pits, complete with oxide membrane covers, are shown to initiate at these off axis facets. The oxide membranes possess remnant signatures of the pore clusters identifying the pore clusters as the structural entity responsible for pit initiation in this system. The role of defect chemistry within the passive oxide in creating these structures is discussed.

Experimental

Aluminum films were sputter deposited (Endura system, Applied Materials) onto a titanium nitride:titanium overlayer on Si(100) wafers. Film growth at 20 $nm \cdot s^{-1}$ and a substrate temperature of 175°C nm was used to produce Al(111) textured films with a nominal grain diameter of 700 nm. The initial surface oxide is formed through O_2 exposure in ambient air at room temperature. This oxide is referred to as an anhydrous model oxide to distinguish it from the native oxide formed with water exposure after mechanical polishing of a bulk Al sample. The observed electrochemical properties of this air-formed oxide, as measured in voltammetry, chronopotentiometry, and in impedance spectroscopy, are nearly identical to those measured for an oxide derived from pure O_2 exposure of an atomically clean Al surface.

Galvanostatic polarization experiments were conducted on individual 0.8 to 3 $x10^{-6}$ cm^2 areas of these Al films using laser drawn quartz capillaries. The capillary tip was coated with a thin layer of silicone (Dow Corning 3140) to serve as an elastomeric seal yielding capillary inner diameters of 10 to 20 μm. The capillary was attached to a polycarbonate cell containing a Ag/AgCl reference electrode and a Pt counter electrode. This cell was mounted to a 3-axis stepper motor controlled positioner and instrumented with a load cell to measure and control contact force between capillary and sample surface. Open circuit potential measurements and anodic polarization were conducted with a low noise, high precision potentiostat (battery powered Jaissle IMP 83 PCT-BC) with the cell in a Faraday cage. Potential measurements were made at 18 Hz. Individual sites were allowed to equilibrate for 30 or 60 minutes in the 50 mM NaCl (pH 7.0) electrolyte prior to anodic polarization. Polarization was conducted using current values ranging from 7 to 45 pA to achieve current densities of 4 to 14 $\mu A \cdot cm^{-2}$ depending on capillary diameter. Current output calibration with a precision 100 GΩ resistor (1%, Ohmite) exhibited an accuracy to within 2% over this current range. Individual sites were rinsed immediately after completing the polarization experiment by micropipetting a water droplet onto the site followed by a gentle flow of N_2 to blow the droplet off the sample surface and to dry the region. Scanning electron microscopy (SEM) analysis was conducted on a FEI Magellan microscope using a monochromatic primary beam at

incident energies ranging from 250 eV to 20 keV. Transmission electron microscopy (TEM) imaging was conducted on a Phillips/Technai F30-ST microscope using a 300 keV electron beam and sample preparation methods as previously reported (11).

Results and Discussion

Single pit initiation events can be galvanostatically driven in a model passive oxide on aluminum. Figure 1a shows the resulting chronopotentiometric response induced by a 9 pA (4 $\mu A \cdot cm^{-2}$) anodic step applied for approximately 740 s. The experimental strategy is to galvanostatically drive the region to the first observed occurrence of a breakdown event and then immediately turn off the applied current to effectively quench any subsequent activity. The overall potential-time response is characteristic of that observed for electrode areas ranging from $8x10^{-7}$ cm^{-2} (10 μm diameter) to $8x10^{-3}$ cm^{-2} (1 mm diameter). Response attributes include: 1) a rapid transition from an equilibrium (open circuit) to an anodic potential as current is first applied at 130 s due to non-faradaic charging, 2) a subsequent gradual increase in potential as the oxide evolves, for example with growth (13), resulting in a larger electric field being required to sustain the applied current, 3) the appearance of a potential maximum, and 4) an eventual decay in the potential as evolving properties of the film facilitate ionic transport at lower field (13). Two discharge events are detected within this potential profile at 175 and 858 s; events where the interface is momentarily depolarized and the potential drops rapidly and then recovers on a longer time scale. Such potential transients have been reported for passive metals undergoing pitting under open circuit conditions and signal the initiation, growth, and repassivation of pits (14,15). The transients detected in Fig. 1a result from the localization of a significant fraction of the applied current at the point of pit initiation up to the point of repassivation. The gradual variation in potential has been subtracted from this trace, using a polynomial fit to the data, and the difference is displayed in Figure 1b highlighting these two events as well as some higher frequency perturbations in potential over the course of this experiment. The recovery of electrode potential from the first event at 175 s is evident in this difference plot. The larger, second event at 858 s results

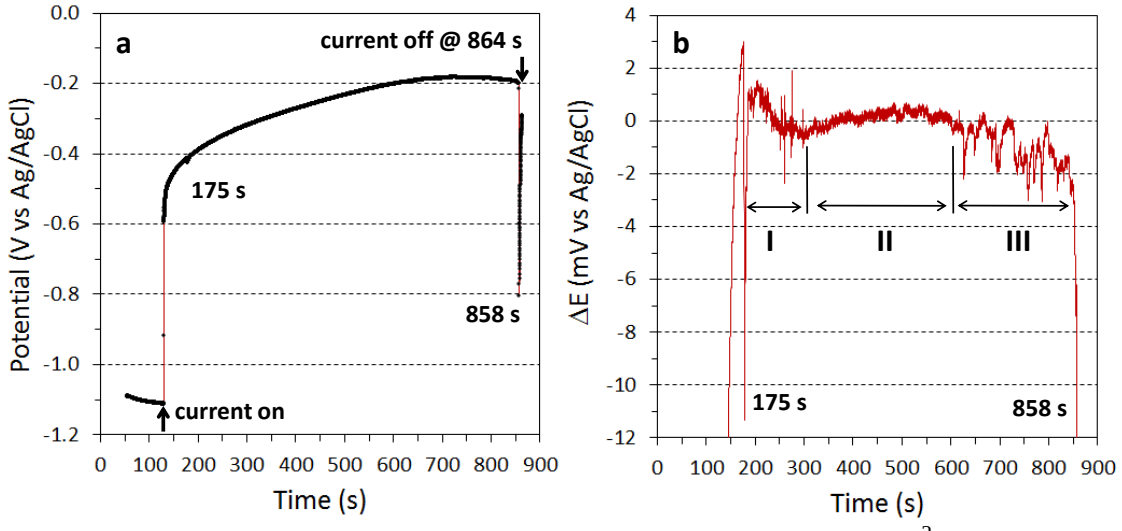

Figure 1. Chronopotentiometric curve produced by applying 4 $\mu A \cdot cm^{-2}$ anodic current to an aluminum thin film (a). The difference (ΔE) in instantaneous and the gradual variation in potential highlights lager amplitude discharge events and smaller potential perturbations (b).

from a greater degree of current localization, suggestive of the formation of a larger pit (15). The applied current was turned off at 864 s during the repassivation of this second event. The potential difference trace demonstrates that smaller scale variation in localized activity occurs along with these larger pit initiation events. Specifically, three distinct regions of electrochemical noise are apparent: (I) an approximate 140 s period after the first event characterized by numerous ±2 mV spikes, (II) a subsequent 300 s period of ±100 μV signal indicating minimal localized activity, and (III) a final 200 s period of approximately -2 mV amplitude transients. At this stage, the relationship between the larger individual breakdown events and the smaller potential fluctuations is not understood. For example, one might hypothesize that the final set of small transients (III) actually signals the initiation of the final pitting event. However, examination of numerous potential traces shows that not all discharge events are preceded by a period of enhanced activity. Irrespective of how these activity signatures are correlated, the demonstrated ability to drive a single breakdown event creates the possibility of characterizing the corresponding local structural and compositional changes produced by this event. Capturing the impact of sufficiently early stage events is expected to yield information as to the origins of pit initiation.

Two classes of oxide breakdown sites are observed in subsequent microscopic analysis of polarized sites. The anodically polarized region described in Figure 1 was mapped using secondary electron microscopy to determine whether specific breakdown sites could be identified. Figure 2a and 2b shows two sites that were found during SEM mapping that could readily be distinguished from the surrounding matrix. The image in Figure 2a shows that a pit has formed and has grown laterally into two grains that share a common grain boundary. Pit growth has presumably been facilitated by an oxide membrane that remains intact over the top of the pit allowing for the development of a sufficiently acidic environment within the enclosed pit to retard regrowth of a passivating oxide. This image was acquired using an incident energy of 250 eV (through a deceleration method) to enhance the overall signal originating from the membrane. Low incident energy electrons do not create appreciable backscattered electrons as an

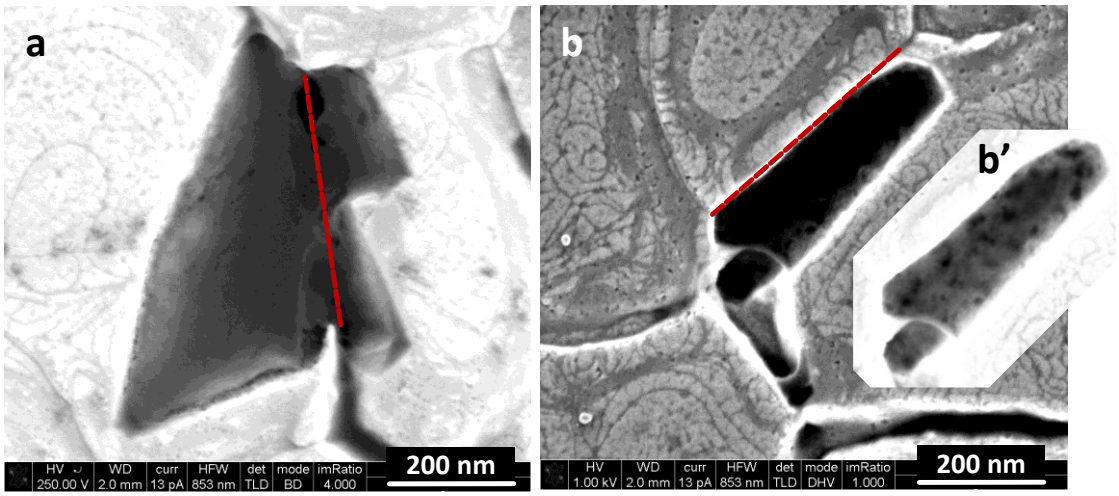

Figure 2. The two sites of localized anodic activity identified using SEM from the polarization of Figure 1. Dashed lines denote the position of a grain boundary. The inset (b') shows a contrast enhanced image of the site of interest.

additional source of secondary electrons, preserving both near surface information and high spatial resolution. The low energy image of Figure 2a shows the presence of a nearly continuous oxide membrane with perforations at discrete positions along the remnant grain boundary between the two grains into which the pit propagated. The second breakdown site, as shown in Figure 2b, appears to be the precursor to a fully nucleated pit being substantially smaller in size than the previous pit of Figure 2a. This structure has formed on one side of a grain boundary (upper diagonal in the image) and possesses a highly perforated or porous appearing membrane, as imaged at 1 keV. Based on feature size, a reasonable hypothesis is that the low magnitude, early time discharge event (175 s) produced the pit precursor of Figure 2b while the large magnitude, longer time discharge event (858 s) produced the pit of Figure 2a. Such a one-to-one correlation between the magnitude of electrochemical events and microscopically characterized sites is currently not available from this experimental work; however, trends are present in these experiments that provide mechanistic details about the events that lead to pit formation.

These pit initiation signatures can be readily reproduced. Figure 3 shows a series of chronopotentiometric curves generated using a range of applied current density values from 4 to 14 $\mu A \cdot cm^{-2}$. The resulting curves show the occurrence of a significant oxide breakdown event after polarization for a sufficient period of time. The time necessary for a breakdown event scales inversely with the applied current density. This latter observation is consistent with an induction time necessary for the formation of critical conditions within the passive oxide that leads to its eventual breakdown. An induction time for pit nucleation has been experimentally demonstrated for a range of passive metals and more relevantly for Al (16).

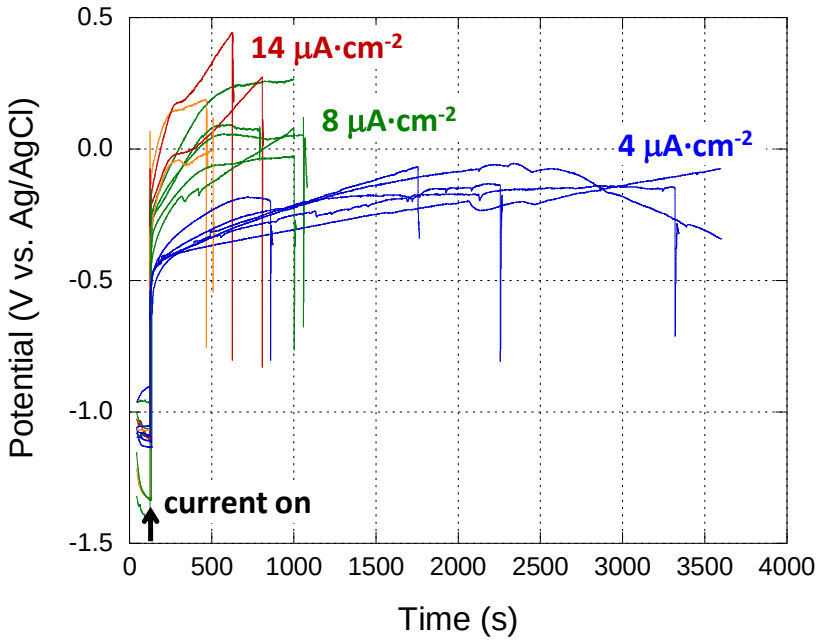

Figure 3. Chronopotentiometric curves produced by applying 4 to 14 $\mu A \cdot cm^{-2}$ anodic current to an aluminum thin film. Individual experiment was terminated prior to or at the occurrence of a single pit initiation event.

Structural characterization of pits generated with galvanostatic polarization provides new information about the critical conditions necessary for oxide breakdown. Figure 4a-c shows images of pits formed at three separately polarized regions depicted by the measurements of Figure 3. As discussed previously, oxide membranes are a common attribute of galvanostatically driven pits and often only fragments or collapsed membranes are observed. For the purpose of developing an understanding of pit initiation, attention is given to three pits from three different sites where the oxide membrane was left intact. The image of the pit in Figure 4a exhibits an oxide membrane that is connected around the perimeter of the pit, but has been breached at the left side of the image. The membrane has deflected into the pit cavity. The downward deflection requires a higher than normal primary energy (5 keV vs. 250 eV) to capture more of the details of the membrane structure. The dominant lateral growth of this pit is toward the interior of a large grain at the base of the image and crystallographic attack of two vertical facets formed the acute angle of the advancing pit perimeter at the image base. The oxide over this portion of the pit exhibits the morphology of the oxide on the surrounding (111) terrace indicating that it is original passive oxide that becomes suspended due to the undercutting dissolution of the grain. Given the growth direction of this pit, initiation occurred in the upper, right quadrant of the image in proximity to a grain boundary (dashed line). This portion of the membrane displays a set of pores, distributed along the arc accent, which likely represents the area where the passive oxide was originally disrupted leading to initiation of the pit. The intact oxide membrane over the pit shown in Figure 4b from a second polarized region possesses a concentrated cluster of pores (circled region) at the center, right of the pit in close proximity to a grain boundary. The presence of this cluster offers strong evidence that the oxide membrane can retain a structural signature of the area of initiation. In Figure 4c, the pit from a third polarized region is shown whose oxide membrane exhibits clusters of pores (indicated by arrows) on either side of grain boundary. The larger holes observed at the upper and lower triple points (original grain boundary lies along a connecting line between these features – see Figure 2a) could be the result of mechanical damage incurred by the membrane.

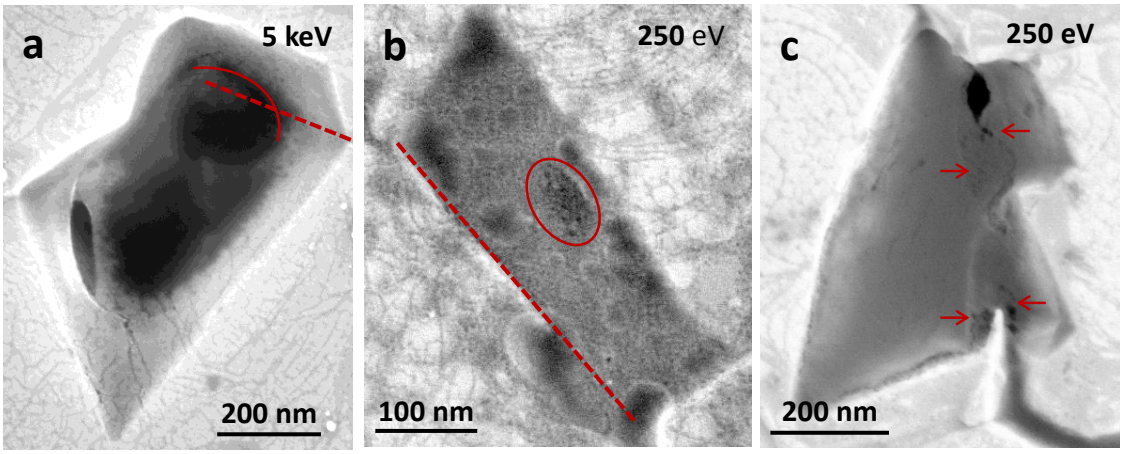

Figure 4. Secondary electron images of pits generated at three separate regions subjected to galvanostatic polarization displaying the presence of pore clusters within the oxide membrane. Pore cluster locations are indicated by curve and arrow accents, while the dashed lines indicate probable position of grain boundaries. Figure 4c is a contrast enhanced image of the same pit shown in Figure 2a.

Structural details extracted from each of these images indicate that fully formed pits initiate in proximity to the grain boundaries, at sites where clusters of pores have formed, and the pore cluster acts as the initiation site for pitting.

The actual site of pit initiation is not necessarily the grain boundary. A more thorough examination of the impact of polarization shows that pore clustering takes place along the off-(111) axis facets between the Al(111) terraces and the actual interface between adjacent grains. This relationship is evident in that the porous membrane precursor imaged in Figure 2b lies off of the grain boundary and is further demonstrated by the images displayed in Figure 5a-c. Figure 5a shows a circular cluster of pores that has formed on one of these facets. The actual interface between the grains (arrow accents) lies below this cluster, although the cluster crosses the boundary. A second, poorly resolved cluster appears to be present on the facet of the lower grain that extends upward in the image toward the grain boundary. A lower density of pores is also present elsewhere on these facets that emerge from the grain boundary, as well as on the adjoining (111) terraces. Figure 5b shows a second common structure observed where pore clusters develop over localized areas with a greater extension onto the lower terrace.

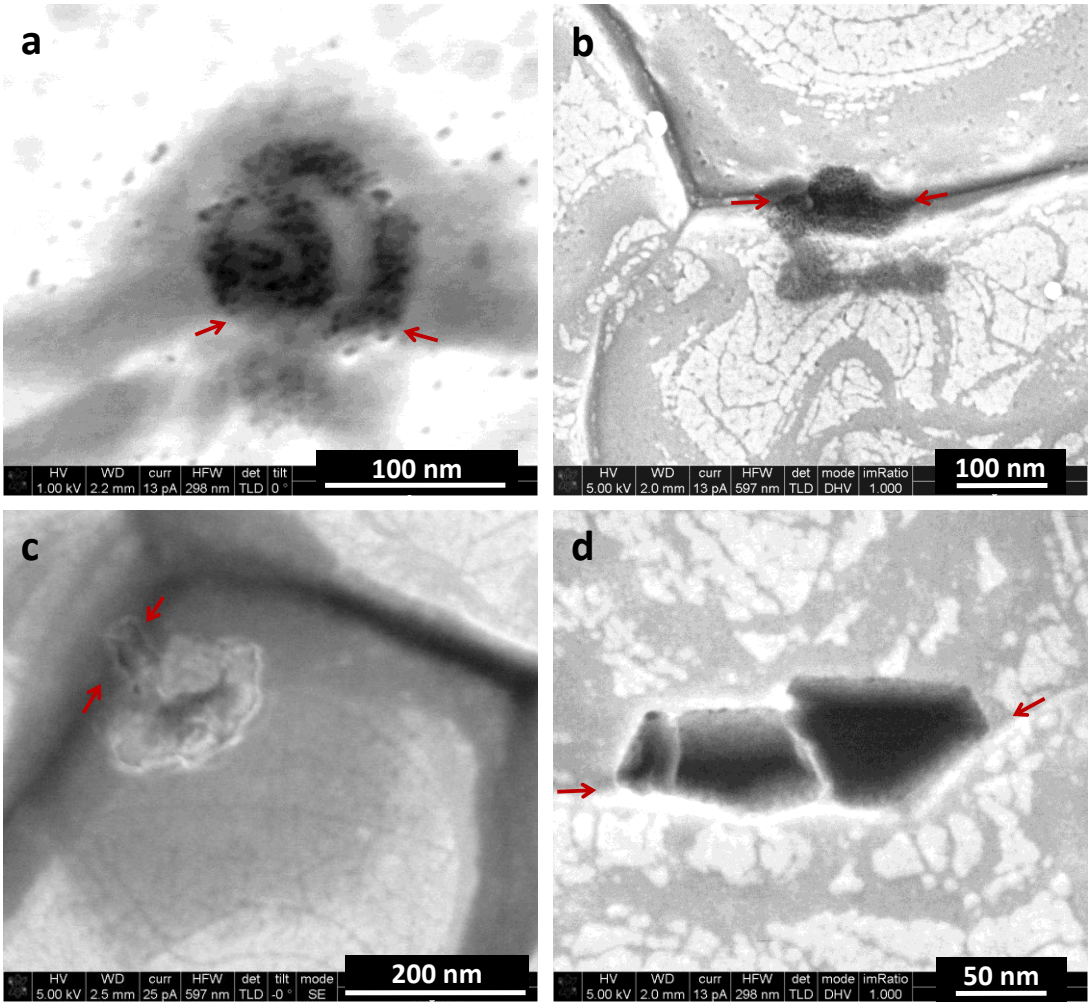

Figure 5. Secondary electron images of pit nucleation sites and nanoscale pits. Arrows denote local tangent of the grain boundary or a boundary between terraces.

Isolated pores also decorate the facets emergent from the grain boundaries in this image. Structures that indicate a greater degree of disruption of the grain surface are also observed, as shown in Figure 5c. This region of concentrated dissolution activity is again centered on the facet emanating from a grain boundary, with only a small extension intersecting the boundary between the upper and lower grains. The pit complex shown in Figure 5d is not located at a grain boundary, but is internal to a large grain. These structures have formed at the boundary of two terraces where the dark contrast oxide is interpreted to be vicinal to the (111) axis. All of these regions exhibit a tendency to form pore clusters and are structurally related to one another due to the fact that off-axis facets will possess a more complex oxide-Al interface structure involving higher step densities (16) and possibly open volume defects in the interfacial oxide.

The origin of pores forming with anodic polarization in the passive oxide on Al has been previously shown to be voids that nucleate at the oxide-Al interface (Figure 6a) and then grow into the oxide (11). A combination of oxygen vacancy accumulation and developed stress at the interface was postulated to be the driver for nucleation. Oxygen vacancy accumulation results from the oxidation of an Al atom and its subsequent incorporation into the disordered lattice of the amorphous oxide (4). The impact of the high rate of oxygen vacancy production in these galvanostatic experiments is to drive vacancy saturation at the most susceptible sites. The high step density and the resulting lower barrier for ionization of Al (reduced coordination at the step) makes these off-(111) axis facets the most likely sites for early stage oxygen vacancy saturation. Enhanced void nucleation is also expected at these sites assuming that the local irregularity in interfacial

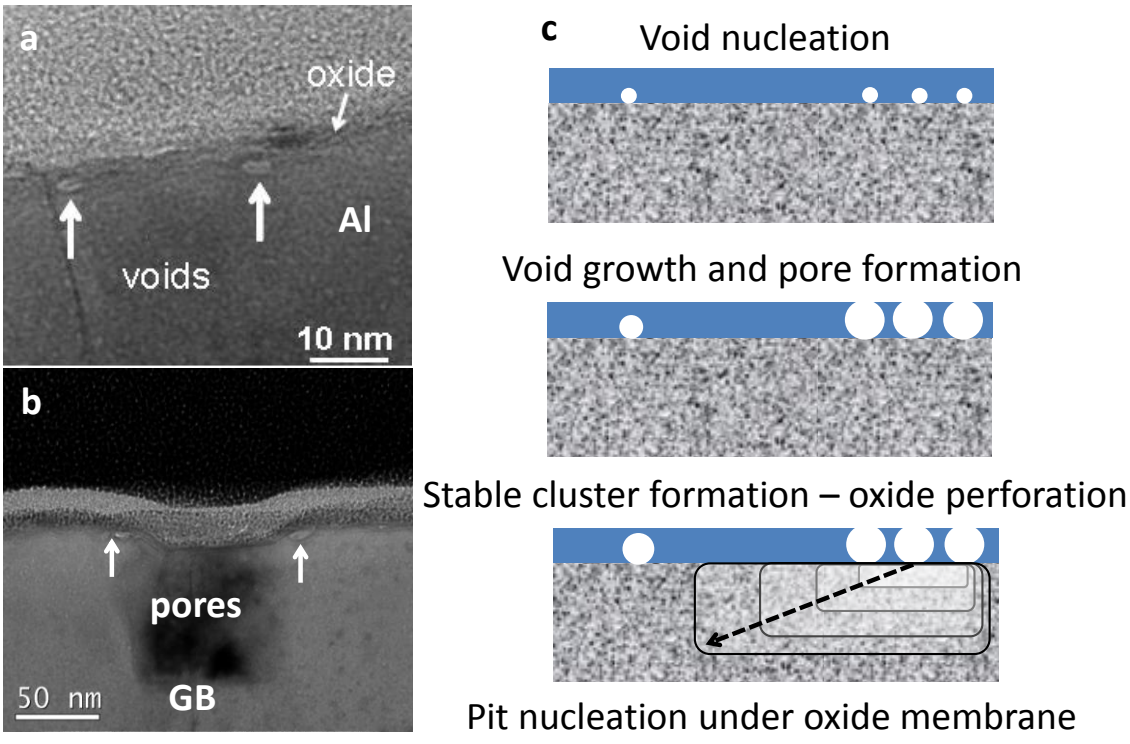

Figure 6. TEM images of galvanostatically polarized electron beam deposited Al(111) films showing interfacial voids (**a**) and pores that have formed on off-(111) facets that extend from the center grain boundary (**b**). A schematic of the process of pore cluster formation and pit nucleation is shown in **c** – arrow denotes progression of pit growth.

structure acts to amplify stress. TEM data from smaller grained (150 nm diameter), electron beam deposited Al(111) films shows that pore clusters often form on these off-axis facets (Figure 6b). Void growth is proposed to occur through the annihilation reaction of anion and cation vacancies at the void nucleation site (11). As a result, the electrochemically more active off-axis facets nucleate and grow voids at higher areal densities and at greater rates than elsewhere on the grain. A schematic view of how voids lead to pit initiation is shown in Figure 6c. Pore formation results from the nucleation and growth of voids into the oxide. Regions of high void density lead to the formation of pore clusters. The pore cluster serves as a pit precursor site that could become a pit nucleus with initiation followed by growth to a fully formed pit. How initiation takes place in the pore cluster is subject to speculation. The breakthrough of any one growing void may present a finite probability of initiation. The cluster may simply increase that probability by the number of voids within the cluster making it more likely that the cluster will give rise to pitting rather than an isolated void in some other location. Such a mechanism would tie pit initiation directly with defect production and reaction rates. Alternately, the oxide may succumb to structural or interfacial failure due to strain amplification at the topologically rough interface of pores penetrating into the substrate at a high local density. For this mechanism, structural flaws are the agent of failure, but initiation would still be determined by defect production and reaction rates. The fact that pit initiation precursor sites (Figures 2b and 5a-c) survive polarization to be observed by electron microscopy is consistent with homogeneous nucleation of voids and pores. The rationale is that multiple potential initiation sites are evolving in time, one site leads to the discharge event where the experiment is stopped, and remaining precursor sites are quenched with the elimination of applied current.

Conclusions

This work demonstrates that it is possible to drive single pit initiation in an Al film to study the mechanistic origins of localized corrosion. Galvanostatic polarization yields an isolated large amplitude potential transient while subsequent scanning electron microscopy identifies the presence of a fully formed pit within the polarized region. Pit initiation occurs preferentially on off-(111) axis facets that are either emergent from the grain boundary or are present at the boundary between (111) terraces on the grain surface. These facets are shown to possess clusters of pores produced by the anodic polarization. Oxide membranes on fully formed pits are shown to possess structural signatures of these pore clusters. Evidence is also found for early stage pore-perforated oxide membranes prior to the formation of a recognizable pit. We conclude from these results that pitting in these films is initiated at the site of these clusters of pores on off-(111) axis facets. We propose that pore clusters originate from point defect chemistry involving oxygen vacancy saturation at off axis facets and the cation-anion vacancy reaction leading to void nucleation, growth, and pore formation. The prevalence of void and pore formation in single and poly-crystalline bulk aluminum suggests that void and pore formation are a generalized precursor for pit initiation in aluminum (11).

Acknowledgements

Al thin film samples were graciously supplied by J.E. Stevens (Sandia National Laboratories). TEM sample preparation by M.J. Rye (Sandia National Laboratories), TEM samples analysis by P.G. Kotula (Sandia National Laboratories), SEM analysis

provided by R.P. Grant (Sandia National Laboratories) and experimental support by M.A. Martinez (Sandia National Laboratories) are gratefully acknowledged. This work was funded by the United States Department of Energy, Office of Basic Energy Sciences, Department of Material Science and Engineering.

Sandia National Laboratories is a multi-program laboratory managed and operated by Sandia Corporation, a wholly owned subsidiary of Lockheed Martin Corporation, for the U.S. Department of Energy's National Nuclear Security Administration under contract DE-AC04-94AL85000.

References

1. Z. Szklarska-Smialowska, "Pitting & Crevice Corrosion," NACE International, Houston, TX, (2005).
2. G. S. Frankel, *J. Electrochem. Soc.*, **145**(6), 2186 (1998).
3. H. H. Strehblow, in *Corrosion Mechanisms in Theory and Practice*, P. Marcus, Editor, p. 243, Marcel Dekker, New York (2002).
4. D. D. Macdonald, *Pure Appl. Chem.*, **71**, 951 (1999).
5. E. McCafferty, *Corr. Sci.*, **45**, 1421 (2003).
6. T. Okada, *J. Electrochem. Soc.*, **132**, 537 (1985).
7. A. Seyeux, V. Maurice, and P. Marcus, *Electrochem. Solid-State Lett.*, **12**, C25 (2009).
8. J. O'M. Bockris and L. V. Minevski, *J. Electroanal. Chem.*, **349**, 375 (1993).
9. G. T. Burstein and S. P. Vines, *J. Electrochem. Soc.*, **148**, B504 (2001).
10. S. T. Pride, J. R. Scully, and J. L. Hudson, *J. Electrochem. Soc.*, **141**, 3028 (1994).
11. K. R. Zavadil, J. A. Ohlhausen, and P. G. Kotula, *J. Electrochem. Soc.*, **153**(8), B296 (2006).
12. G. S. Frankel, J. R. Scully, and C. V. Jahnes, *J. Electrochem. Soc.*, **143**, 1834 (1996).
13. K. R. Zavadil, P.G. Kotula, and J.A. Ohlhausen, *ECS Trans.*, **11**(15), 89 (2008).
14. H. S. Isaacs, *Corr. Sci.*, **29**, 313 (1989).
15. M. Hashimoto, S. Miyajima, T. Murata, *Corr. Sci.*, **33**, 905 (1992).
16. F. D. Wall, M. A. Martinez, and J.J. Van Den Avyle, *J. Electrochem. Soc.*, **151**, B354 (2004).
17. R. S. Timsit, W. D. Waddington, C. J. Humphries, and J. L. Hutchison, *Appl. Phys. Lett.* **46**, 830 (1985).